Research Article

Bernd Bauerhenne* and Martin E. Garcia

Universal behavior of the band gap as a function of the atomic mean-square displacement in laser-excited silicon

https://doi.org/10.1515/aot-2019-0063
Received November 27, 2019; accepted May 14, 2020; previously published online June 9, 2020

Abstract: We performed systematic *ab-initio* molecular dynamics (MD) simulations of fs-laser-excited silicon (Si) using the T_e-dependent density functional theory (DFT). We considered the case in which the potential energy surface (PES) is strongly modified by the laser excitation, so that nonthermal melting occurs. We analyzed the correlation between the time dependence of electronic properties like the band gap and the laser-induced atomic motion. Surprisingly, we found that the indirect electronic band gap decreases as a universal function of the atomic mean-square displacement (MSD) almost independently of the electronic temperature (laser fluence) and that the dependence is linear for a wide range of MSDs. We also found that a universal dependence is also present when analyzing the band gap as a function of the relative Bragg peak intensities, which can be directly measured in experiments.

Keywords: band gap; fs-laser excitation; silicon.

1 Introduction

Silicon (Si) is the most used semiconductor worldwide. It exhibits an indirect band gap of 1.17 eV between the Γ and the *X* points of the Brillouin zone [1]. The direct gap at the Γ point amounts to 3.42 eV [1]. It is known from high-pressure experiments that the band gaps of Si are very sensitive to external conditions. For instance, applying an external pressure of 20 GPa produces a closure of the band gap and consequently a metalization of Si [2, 3]. This occurs because, under high pressure, the interatomic distance slightly decreases, which leads to an increase of the covalent bond strength (or hopping elements). This, in turn, results in a broadening of the valence and conduction bands, which then overlap.

In gallium arsenide (GaAs), it was theoretically shown that the laser-induced melting induces a collapse of the band gap [4]. Femtosecond (fs)-laser excitation of Si can also lead to a metalization if the laser fluence is high enough. However, the mechanism in this, although also related to atomic displacements, is completely different. The closure of the band gap occurs due to melting. Liquid Si is metallic because it exhibits a larger number of nearest neighbors than the zinc-blende crystalline structure, thus leading to a broadening of the valence and conduction bands. The metallic character of liquid Si has been experimentally confirmed [5]. The laser-induced melting and consequent metalization of Si were predicted by Stampfli and Bennemann in 1994 [6] using the tight binding theory and by Silvestrelli and Parrinello in 1996 [7] using electronic-temperature-dependent density functional theory (DFT).

Now, based on the aforementioned facts, one can conclude that the band gap of Si closes upon a tiny displacement of the atoms or upon a big rearrangement of the atomic environment. One can expect that simultaneous small displacements and rearrangements, as it happens during the first stages after laser excitation, will produce a reduction of the band gap in Si. It is, however, not yet known how the band gap behaves as a function of the combined action of displacement and rearrangement during laser-induced melting. An appropriate quantity to measure the degree of atomic motion and structural rearrangement is the atomic mean-square displacement (MSD), which has also the advantage that it can be accessed through, for instance, the measurement of time-dependent Bragg peak intensities in time-resolved crystallographic experiments [8, 9].

***Corresponding author: Bernd Bauerhenne,** Theoretical Physics II Group and Center for Interdisciplinary Nanostructure Science and Technology (CINSaT), University of Kassel, Heinrich-Plett-Str. 40, 34132 Kassel, Germany, e-mail: bauerhenne@uni-kassel.de. https://orcid.org/0000-0002-3397-2290
Martin E. Garcia: Theoretical Physics II Group and Center for Interdisciplinary Nanostructure Science and Technology (CINSaT), University of Kassel, Heinrich-Plett-Str. 40, 34132 Kassel, Germany

In this paper, we predict that the band gap of Si exhibits a universal behavior as a function of the MSD upon non-thermal laser-induced melting almost independent of the laser intensity. Moreover, the band gap depends linearly on the MSD in a relatively large interval. Plotted as a function of the intensity of different Bragg peaks, the band gap can be represented by a universal function. The findings of this work might trigger pump-probe experiments to confirm the prediction.

The paper is organized as follows. Section 2 describes the simulation method. We explain the physical picture of a fs-laser excitation, the modeling by electronic-temperature-dependent DFT and our simulation code CHIVES (Code for Highly excIted Valence Electron Systems). In Section 3, we present the results of our molecular dynamics (MD) simulations of fs-laser-excited Si. We show that an intense fs-laser excitation melts Si in less than 100 fs and that the electronic band gap vanishes during this process. Furthermore, we show that the band gap is a universal function of the atomic MSD or of the relative Bragg peak intensity. We finish the paper with Section 4, where we discuss or results.

2 Simulation method

2.1 Physical picture of fs-laser excitation

Intense fs-laser pulses mainly excite the electrons in a solid, whereas, in most cases, the ions remain initially mainly unaffected. The fs-laser field excites in semiconductors a significant amount of electrons from the valence band into the conduction band, so that hot electron hole pairs are created. Through intraband scattering and interband Auger processes, a fast thermalization of the electrons and holes occurs within a timescale of 10–50 fs. After the thermalization, the electrons and holes form a Fermi distribution with a common chemical potential μ_{eh} at a high temperature T_e [10, 11]. In this so-called one-μ model, T_e is an input parameter that controls the laser-excitation strength. A different model for describing the thermalized electron hole pairs was developed by Tangney and Fahy [12]: They assume that the intraband thermalization is fast and the interband thermalization needs a much longer time, so that the electrons and holes are not in equilibrium. They further assume that the electrons and holes have the same temperature T_e, but different chemical potentials, namely μ_e and μ_h. In this so-called two-μ model, the temperature T_e and the fraction n_{ex} of excited electron hole pairs are input parameters. In Figure 1, both

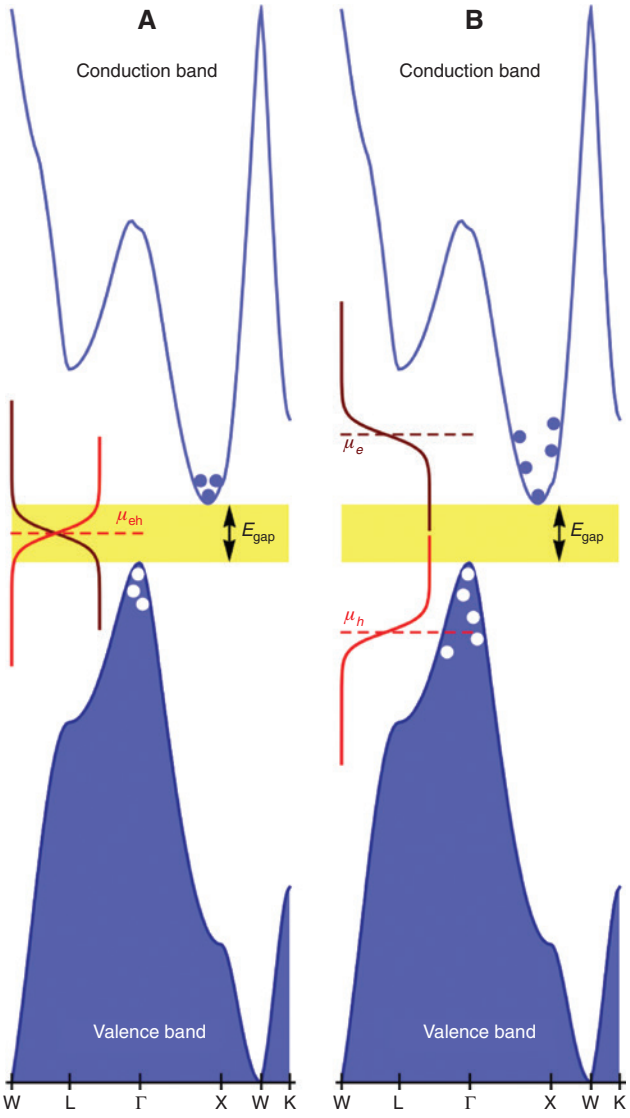

Figure 1: Illustration of the two-μ model (A) and the one-μ model (B). For description see text.

models are illustrated using the *ab-initio* electronic band structure of Si obtained from the DFT code WIEN2k [13]. The state described by the one- or two-μ model far away from the thermal equilibrium with hot electrons and cold ions decays via incoherent electron-ion scattering on a picosecond (ps) timescale.

The electrons are responsible for the interatomic bonding. Following the Born-Oppenheimer approximation, the ions move on a potential energy surface (PES) generated by the electrons. The presence of hot electrons and holes changes dramatically the bonding behavior of the ions, or in other words, changes the PES. As a consequence, the ions feel forces that differ significantly from the forces occurring in the electronic ground state and the ions are accelerated on the laser-excited PES.

2.2 Modeling the effect of hot electrons and holes

The PES generated from thermalized laser-excited electron hole pairs is determined by the Helmholtz free energy F, which reads in T_e-dependent DFT [10]

$$\begin{aligned} F(\{\mathbf{r}_i\}, T_e) &= \sum_{\varepsilon_m} n(\varepsilon_m, T_e)\varepsilon_m + E_{XC}(\rho(\mathbf{r})) \\ &\quad - \int V_{XC}(\mathbf{r})\rho(\mathbf{r})d\mathbf{r} - \frac{1}{2}\int \frac{\rho(\mathbf{r})\rho(\mathbf{r}')}{|\mathbf{r}-\mathbf{r}'|} d\mathbf{r}d\mathbf{r}' \\ &\quad + V_{II}(\{\mathbf{r}_i\}) - T_e S_e. \end{aligned} \tag{1}$$

Here, $\{\mathbf{r}_i\}$ denotes the atomic coordinates and $n(\varepsilon_m, T_e)$ describes the occupation number of the Kohn-Sham energy level ε_m. Within the one-μ model, these occupation numbers are given by a Fermi distribution at temperature T_e:

$$n(\varepsilon_m, T_e) = \frac{2}{e^{\frac{\varepsilon_m - \mu_{eh}}{k_B T_e}} + 1}, \tag{2}$$

where k_B denotes the Boltzmann constant and the chemical potential μ_{eh} is obtained from the conservation of the total number of electrons

$$N_e = \sum_{\varepsilon_m} n(\varepsilon_m, T_e). \tag{3}$$

The factor 2 in Eq. (2) accounts for the spin-up and -down electrons. Within the two-μ model, the occupation numbers of the holes in the valence band and of the electrons in the conduction band are given by individual Fermi distributions with different chemical potentials μ_h, μ_e and the same temperature T_e:

$$n(\varepsilon_m, T_e) = \begin{cases} \dfrac{2}{e^{\frac{\varepsilon_m - \mu_h}{k_B T_e}} + 1}, & \varepsilon_m \le \varepsilon_F \\ \dfrac{2}{e^{\frac{\varepsilon_m - \mu_e}{k_B T_e}} + 1}, & \varepsilon_m > \varepsilon_F \end{cases} \tag{4}$$

Here, the states below the Fermi energy ε_F are referred to the valence band and the states above the Fermi energy ε_F are referred to the conduction band. The two chemical potentials μ_h, μ_e are obtained from the two conditions that the total number of electrons (3) and that the given fraction n_{ex} of excited electrons are reached:

$$n_{ex} N_e = \sum_{\varepsilon_m > \varepsilon_F} n(\varepsilon_m, T_e). \tag{5}$$

Furthermore, in Eq. (1), ρ is the electronic charge density

$$\rho(\mathbf{r}) = \sum_m n(\varepsilon_m, T_e)\varphi_m^*(\mathbf{r})\varphi_m(\mathbf{r}) \tag{6}$$

with $\varphi_m(\mathbf{r})$ being the Kohn-Sham orbitals. E_{XC} denotes the exchange and correlation energy and V_{XC} the exchange and correlation potential. V_{II} describes the ion-ion repulsion and S_e is the electronic entropy

$$\begin{aligned} S_e &= -k_B \sum_{\varepsilon_m} (n(\varepsilon_m, T_e)\log(n(\varepsilon_m, T_e)) \\ &\quad + (1 - n(\varepsilon_m, T_e))\log(1 - n(\varepsilon_m, T_e))). \end{aligned} \tag{7}$$

The indirect band gap is calculated as the difference between the highest occupied energy level and the first unoccupied energy level at $T_e = 0$. Thus, using the ascending sorted Kohn-Sham energy levels ε_m, the indirect electronic band gap can be calculated from

$$E_{gap} = \varepsilon_{\frac{1}{2}N_e + 1} - \varepsilon_{\frac{1}{2}N_e}, \tag{8}$$

where $\varepsilon_{\frac{1}{2}N_e} = \varepsilon_F$ corresponds to the Fermi energy. The factor $\frac{1}{2}$ accounts that two electrons can occupy one Kohn-Sham energy level due to the spin. For Si, N_e is always an even number, so that $\frac{1}{2}N_e$ is an integer. As Si has got an indirect band gap, one has to consider several $\mathbf{k}$-points for the electrons in the calculations. Using the Helmholtz free energy (1), the force $\mathbf{f}_j$ on atom j, needed for MD simulations, can be calculated just by

$$\mathbf{f}_j = -\nabla_{\mathbf{r}_j} F(\{\mathbf{r}_i\}, T_e). \tag{9}$$

2.3 *Ab-initio* code CHIVES

We perform *ab-initio* simulation of laser-excited solids by using the T_e-dependent DFT code CHIVES [14–18], which was developed in our group. We implemented the local density approximation (LDA) in CHIVES. A benchmark test in Si shows that our code can be more than 200 times faster compared with the free available code ABINIT at the same level of accuracy in simulating the structural response of Si after fs-laser excitation [18].

To achieve an efficient implementation of T_e-dependent DFT, we proceeded as follows: We separated the electrons into core and valence electrons. The atomic nuclei and the core electrons are treated with Goedecker, Teter and Hutter pseudopotentials [19]. The valence electrons are described explicitly by an optimized basis set of atom-centered Gaussian functions of s, p and d type.

The usage of Gaussian functions allows us to use much less basis functions to reach the same accuracy compared to the widely used plane waves. Nevertheless, the drawback of Gaussian functions is the more complicated implementation and that one has to determine the basis set for each individual element separately. Furthermore, we use the so-called order (N) methods [20], where N is the number of treated atoms: The Hartree potential, which corresponds to the fourth term in Eq. (1), and the exchange and correlation potential V_{XC} as well as the electronic charge density ρ are calculated on a fine cubic mesh of grid points without further approximations. The one-μ and two-μ models are implemented to simulate the effects of a fs-laser excitation. 1, 2, 4 or 8 **k**-points can be chosen for the electrons. We implemented the sum over the **k** points using the message passing interface (MPI). We utilized open multi-processing (OPENMP) parallelized computation for the Hamiltonian matrix elements, electronic charge density and the density matrix. The diagonalization is efficiently performed using optimized linear algebra package (LAPACK) subroutines. The Pulay-Kerker mixer is applied in the self-consistent cycle for solving the Kohn-Sham equations, which allows also the treatment of surfaces [16]. Furthermore, the self-consistent cycle is efficiently initialized by using a charge density extrapolation from previous time steps. We implemented the velocity Verlet algorithm to simulate the MD.

3 MD simulations of Si at high T_e

For all presented calculations, we utilized a bulk supercell containing $N_{at}=432$ Si atoms. This supercell consists of $3\times3\times6$ primitive cells. We set periodic boundary conditions in all room directions and used the lattice parameter $a=0.539872$ nm, which we obtained by a lattice parameter optimization of the ideal diamond-like crystal structure at $T_e=316$ K (1 mHa) within the one-μ model. We considered 8 **k**-points for the electrons. We initialized the atoms at an ionic temperature of $T_i=316$ K using real random numbers from https://www.random.org. For this, we utilized the harmonic approximation of the PES, which allows to set directly atomic displacements and velocities compatible to $T_i=316$ K. The approach is described in detail in Zijlstra et al. [21].

Using different sets of random numbers, we generated 12 independent initializations, which we used to get always 12 independent MD simulation runs.

To simulate the influence of a fs-laser pulse, we first utilized the one-μ model and raised T_e to a constant high value and performed MD simulations using a time step of 2 fs. We simulated 0.25 ps, so that we can neglect the effects induced by electron-phonon coupling. The six T_e s, namely 12 631 K (40 mHa), 18 947 K (60 mHa), 25 262 K (80 mHa), 31 578 K (100 mHa), 37 893 K (120 mHa) and 44 209 K (140 mHa), were simulated. In a second step, we used the two-μ model to perform MD simulations of fs-laser excited Si.

3.1 Effects of the high T_e

To measure the disorder of the crystal lattice structure, we use the atomic MSD defined by

$$\mathrm{MSD}(t)=\frac{1}{N_{at}}\sum_{j=1}^{N_{at}}|\mathbf{u}_j(t)|^2, \tag{10}$$

where $\mathbf{u}_j(t)$ denotes the displacement of the j-th atom from its equilibrium position at time t. We finally average the obtained MSD values over the 12 runs:

$$\langle\mathrm{MSD}(t)\rangle=\frac{1}{12}\sum_{k=1}^{12}\mathrm{MSD}_k(t), \tag{11}$$

where $\mathrm{MSD}_k(t)$ denotes the atomic MSD of run k at time t. Due to the presence of hot electrons, the lattice melts ultrafastly for the T_e s 18 947 K, 25 262 K, 31 578 K, 37 893 K and 44 209 K. This can be clearly seen in Figure 2, where the atomic MSD $\langle\mathrm{MSD}(t)\rangle$ averaged over the 12 runs is shown as a function of time. Except for $T_e=12631$ K, the atomic MSD exceed the Lindemann stability limit within 120 fs or faster. Due to the excitation of a significant amount of electrons from bonding to anti-bonding orbitals, the laser-excited PES induces strong forces on the atoms, which are dramatically accelerated, so that the crystal structure is ultrafastly destroyed. In a previous study [22], we found out that

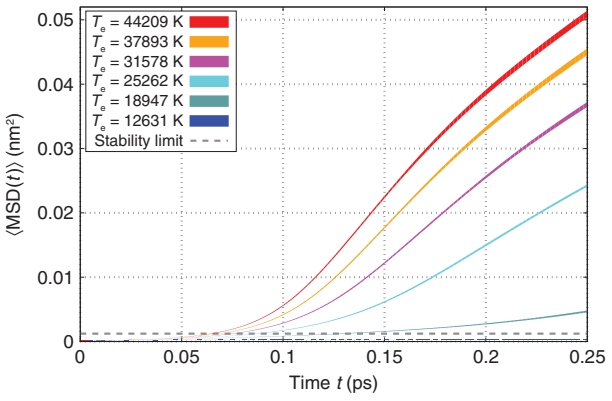

Figure 2: Atomic mean-square displacement is shown as a function of time t averaged over 12 runs at the studied T_es. The thickness of the curves corresponds to the standard deviation between the 12 runs.

$T_e = 17052$ K (54 mHa) is the critical electronic temperature T_e that induces the so-called non-thermal melting.

In experiments, one does not have direct access to the atomic MSD. Moreover, one can measure time-resolved the intensity changes of the Bragg peaks [8, 9]. The Bragg peaks are commonly labeled by the Miller indices h, k, l. The relative intensity of a Bragg peak can be directly calculated from the atomic coordinates $\mathbf{r}_1(t)$, …, $\mathbf{r}_{N_{\text{at}}}(t)$ as

$$I_{hkl}(t) \propto \left| \sum_{j=1}^{N_{\text{at}}} e^{i\mathbf{q}_{hkl}\cdot\mathbf{r}_j(t)} \right|^2 . \tag{12}$$

The related scattering vector

$$\mathbf{q}_{hkl} = h\mathbf{b}_1 + k\mathbf{b}_2 + l\mathbf{b}_3 \tag{13}$$

is constructed from the reciprocal lattice vectors $\mathbf{b}_1$, $\mathbf{b}_2$, $\mathbf{b}_3$ with the help of the Miller indices h, k, l. Here, for Si, the reciprocal lattice vectors form a bcc grid, as the bcc grid is the reciprocal grid of the fcc grid and the diamond-like structure is constructed as a fcc grid with two basis atoms, namely one at $[0, 0, 0]^t$ and one at $\left[\frac{a}{4}, \frac{a}{4}, \frac{a}{4}\right]^t$. Time-dependent Debye-Waller theory [23] allows approximately to connect the intensity decay of the Bragg peaks with the atomic MSD:

$$\frac{I_{hkl}(t)}{I_{hkl}(t_0)} = e^{-\frac{1}{3}|\mathbf{q}_{hkl}|^2(\text{MSD}(t)-\text{MSD}(t_0))} . \tag{14}$$

Here, t_0 denotes the start time of the MD simulation. In the top panel of Figure 3, we show the time-dependent relative intensities of the (111), (220), (311) and (400) Bragg peaks directly calculated from the atomic coordinates using Eq. (12) averaged over 12 runs at $T_e = 25262$ K. The dashed curves indicate the time behavior of these Bragg peaks obtained from the atomic MSD using the Debye-Waller theory (14). In the bottom panel of Figure 3, we show the time-dependent intensity of the (111) Bragg peak at all studied T_e s averaged over 12 runs. Again, the dashed curve indicates the time behavior obtained from the Debye-Waller theory.

In Figure 3, we can clearly see that time-dependent Debye-Waller theory describes accurately the intensity decay of the Bragg peaks. Only at very low peak intensities, a small mismatch occurs. Equation (14) indicates that Bragg peaks related to a bigger scattering vector $\mathbf{q}_{hkl}$ decay faster with increasing atomic MSD and, consequently, decay faster to zero, which can also be seen in the top panel of Figure 3.

Now, we study the influence of a fs-laser excitation on the indirect electronic band gap. Figure 4 shows the indirect electronic band gap $\langle E_{\text{gap}}(t)\rangle$ as a function of time t. Again, we averaged the band gap similar to the atomic MSD over the 12 runs. The increase of T_e firstly increases the indirect band gap. Then, the band gap decreases monotonously to zero for T_es above the non-thermal melting threshold. For $T_e = 12631$ K below the non-thermal melting threshold, it decreases slightly at first and then remains almost constant.

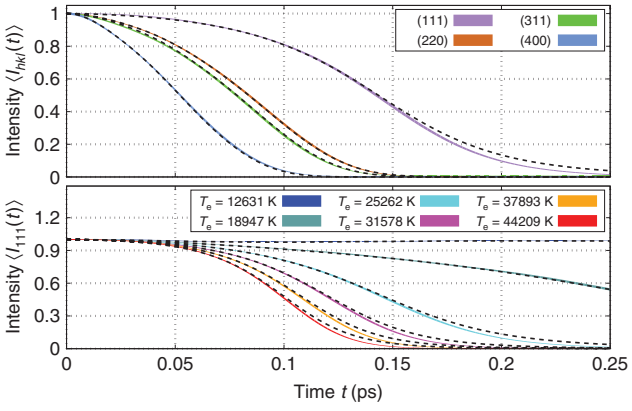

Figure 3: Top panel: Relative intensity of selected Bragg peaks is shown as a function of time t averaged over 12 runs at $T_e = 25262$ K. Bottom panel: Relative intensity of the (111) Bragg peak is shown as a function of time t averaged over 12 runs at the studied T_es. The colored solid curves are directly calculated from the atomic coordinates and the black dashed curves are obtained from the time-dependent Debye-Waller theory.

3.2 Correlation between band gap and atomic displacements

To further analyze the behavior of the indirect electronic band gap, we plot it as a function of the atomic

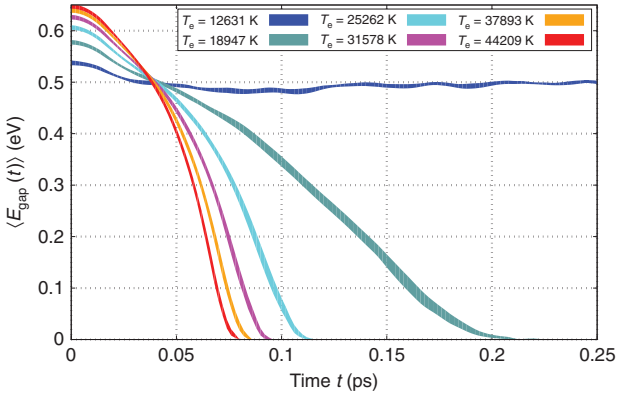

Figure 4: Indirect electronic band gap is shown as a function of time t averaged over 12 runs at the studied T_es. The thickness of the curves corresponds to the standard deviation between the 12 runs.

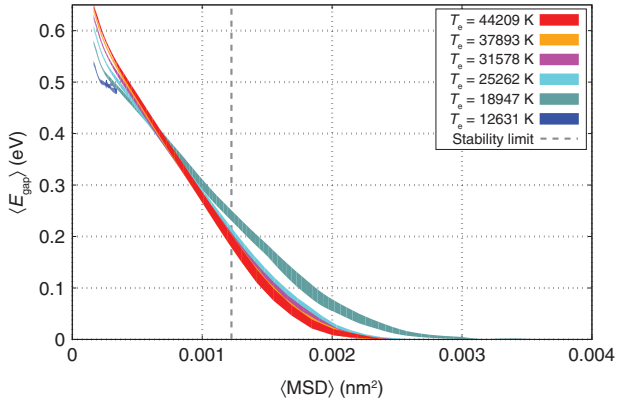

Figure 5: Indirect electronic band gap is shown as a function of atomic mean-square displacement averaged over 12 runs at the studied T_es. The thickness of the curves corresponds to the standard deviation between the 12 runs.

MSD averaged over 12 runs in Figure 5. The thickness of the curves correspond to the standard deviation between the 12 runs. Figure 5 indicates that there exists an **universal** relation between the band gap and the atomic MSD almost independent of T_e. In addition, this dependency is approximately linear for a wide range of atomic MSDs. We conclude that the actual value of the band gap depends only on the atomic MSD and is almost independent on the laser fluence. In addition, the band gap is highly sensitive to atomic displacements, as it disappears already at an atomic MSD of 0.003 nm², where the crystal structure is still recognizable. We can clearly see this in Figure 6, where the Si supercell is shown for an atomic MSD of 0.003 nm² and 0.0002 nm², which corresponds to the atomic structure before the laser excitation. In addition, we showed the atomic structure for an atomic MSD of 0.02 nm², where the crystal structure is clearly molten.

Indeed, the increase of the atomic MSDs from 0.0002 nm² to 0.0030 nm² changes significantly the electronic density of states, which can be seen in Figure 7, where the latter is shown for both MSDs at $T_e = 18947$ K.

3.3 Correlation between band gap and Bragg peak intensities

If we plot the indirect electronic band gap, which is directly measurable in experiments [24], as a function of the relative Bragg intensity, which is also directly available in experiments, we again obtain a universal behavior approximately independent of T_e, as it can be seen in Figure 8 for the studied Bragg peaks. Moreover, the dependency is again approximately linear for a wide range of relative Bragg peak intensities for all considered peaks.

Bragg peaks related to a smaller scattering vector $\mathbf{q}_{hkl}$ decay slower with increasing atomic MSD. Therefore, for such Bragg peaks, the indirect band gap decays faster to zero as a function of the relative peak intensity compared to Bragg peaks with bigger scattering vectors.

We want to note that, besides the study of bragg peak intensities, the electron thermalization following a fs-laser excitation can be directly measured using electron or photon spectroscopy [24].

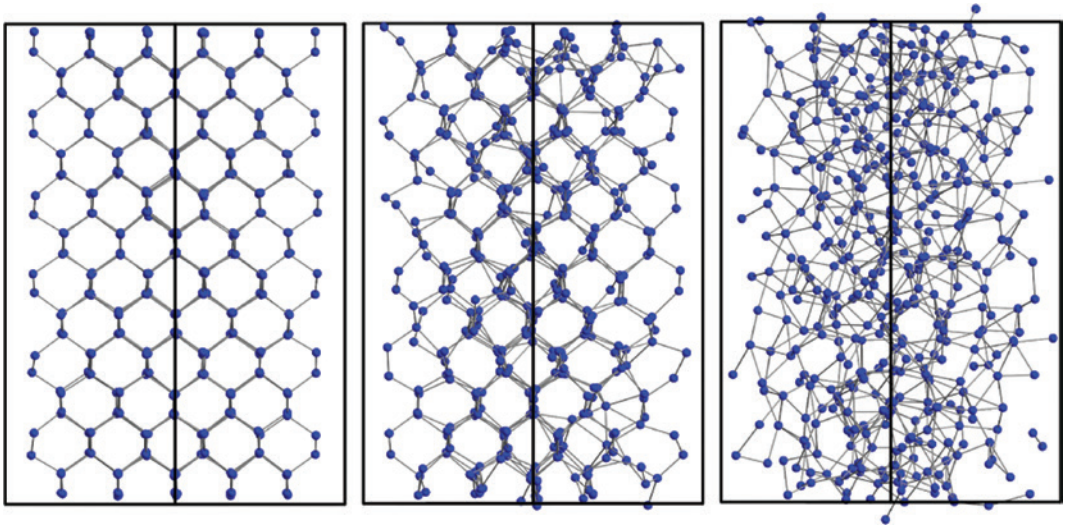

Figure 6: 432-Atom Si supercell projected in the [110]-direction is shown for an atomic mean-square displacement (MSD) of 0.0002 nm² (left), 0.003 nm² (middle) and 0.02 nm² (right).

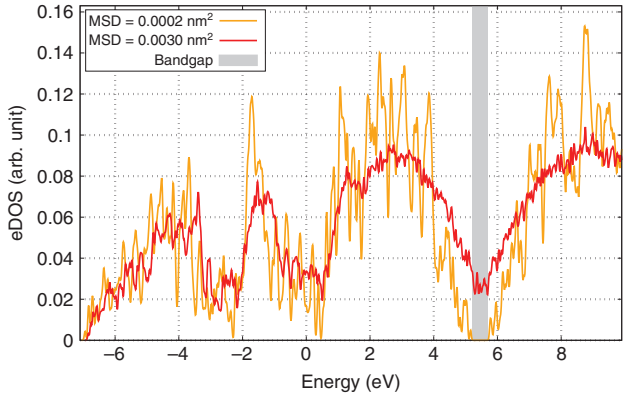

Figure 7: Electronic density of states (eDOS) is shown at $T_e = 18947$ K for an atomic mean-square displacement (MSD) of 0.0002 nm² and 0.003 nm². The band gap at MSD = 0.0002 nm² is highlighted in gray.

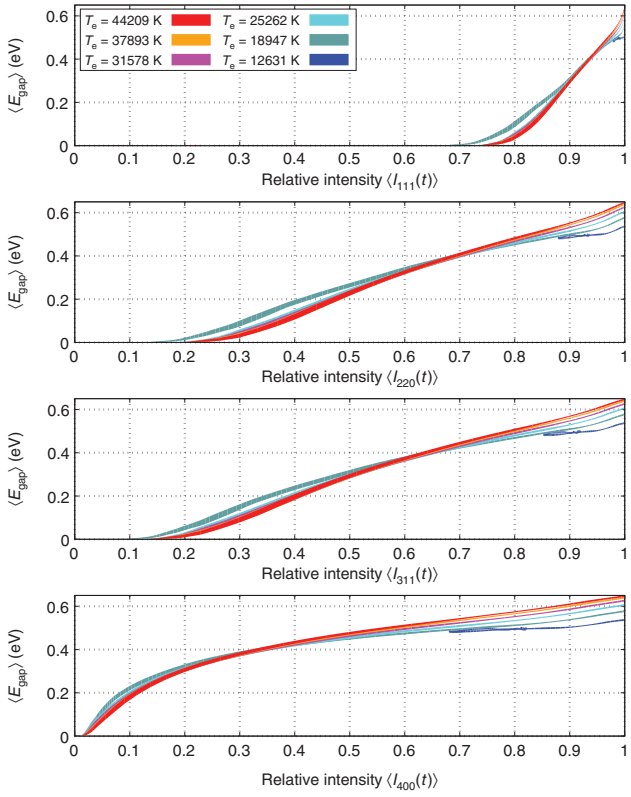

Figure 8: Indirect electronic band gap is shown as a function of the relative Bragg peak intensity averaged over 12 runs at the studied T_es. The thickness of the curves corresponds to the standard deviation between the 12 runs.

3.4 Results obtained from the two-μ model

We considered $n_{ex} = 14.14\%$ excited carriers, which correspond approximately to the fraction of excited carriers within the one-μ model at $T_e = 25262$ K, and performed MD simulations within the two-μ model at various T_e s, namely 316 K, 12 631 K, 18 974 K and 31 578 K. We utilized the same initial conditions as before and performed again at each temperature T_e 12 independent runs. In Figure 9, we present the indirect electronic band gap as a function of the atomic MSD for the different T_es and $n_{ex} = 14.14\%$ within the two-μ model. We also show the curve obtained within the one-μ model at $T_e = 25262$ K with approximately $n_{ex} = 14.14\%$.

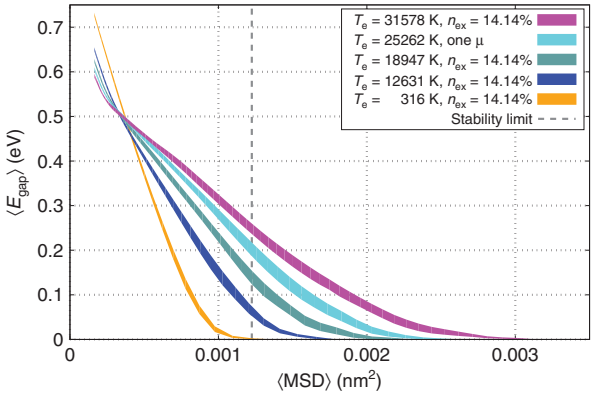

Figure 9: Indirect electronic band gap is shown as a function of atomic mean-square displacement averaged over 12 runs for different T_e s and $n_{ex} = 14.14\%$ obtained from the two-μ model compared with $T_e = 25262$ K obtained from the one-μ model. The thickness of the curves corresponds to the standard deviation between the 12 runs.

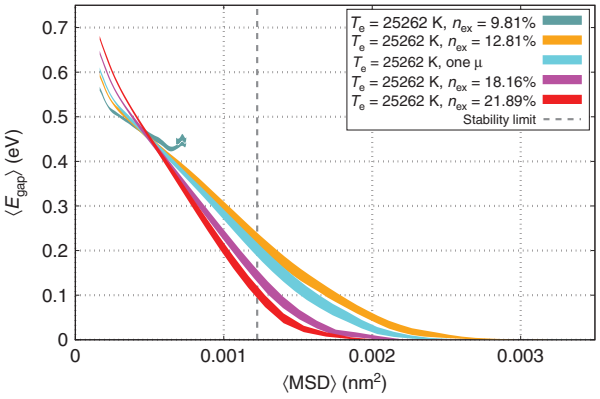

Figure 10: Indirect electronic band gap is shown as a function of atomic mean-square displacement averaged over 12 runs for different n_{ex} s and $T_e = 25262$ K obtained from the two-μ model compared with $T_e = 25262$ K obtained from the one-μ model. The thickness of the curves corresponds to the standard deviation between the 12 runs.

In addition, we considered $T_e = 25262$ K, at which approximately $n_{ex} = 14.14\%$ of the carriers are excited within the one-μ model, and performed MD simulations within the two-μ model at various n_{ex}s, namely 9.81%, 12.81%, 18.16% and 21.89%. We utilized the same initial conditions as before and performed again at each fixed

fraction of excited carriers n_{ex} 12 independent runs. In Figure 10, we present the indirect electronic band gap as a function of the atomic MSD for the different n_{ex} s and $T_e = 25262$ K within the two-μ model. We also show the curve obtained within the one-μ model at $T_e = 25262$ K with approximately $n_{ex} = 14.14\%$. At $n_{ex} = 9.81\%$, the number of excited carriers is too small to induce a melting of the crystal structure. Consequently, the indirect band gap does not vanish.

Also within the two-μ model, the indirect band gap vanishes after the fs-laser excitation, if the crystal structure melts. But now, the indirect band gap is not a universal function of the atomic MSD as it is the case within the one-μ model.

4 Discussion

The two-μ model explains very well the fs-laser-induced oscillation of the A_{1g} phonon mode in bismuth [25] and TiO_2 [26] compared with experiments at quite low fs-laser excitations, where the crystal structure keeps intact. After the fs-laser excitation, the relaxed electrons in Si are properly described by the one-μ model using a high electronic temperature [7, 11]. Therefore, the two-μ model can only describe very early states of intense fs-laser-excited Si, and the two different μs will soon converge to the same value. Consequently, we expect that the band gap in Si as a function of the atomic MSDs will not follow a universal curve for different laser intensities at very small MSDs, where the two-μ model may be valid, and will then converge to one universal function, as soon as one chemical potential for electrons and holes is reached. The time-resolved measurement of the band gap and the Bragg peak intensity at different laser fluences could confirm the universal behavior of the band gap. Moreover, such an experimental setup may also determine at which MSD the convergence to a universal curve will occur. The latter will indicate the point, where the joint thermalization of electrons and holes is finished and the one-μ model is valid.

Our simulations are based on DFT within the LDA. It is well known that LDA generates too small band gaps in semiconductors compared to experiments [27]. We obtain an indirect band gap of 0.48 eV at 316 K, whereas the experimental value of the indirect band gap at 316 K is 1.12 eV [28]. In addition, LDA predicts an increase of the band gap at increasing T_e, as one can see in Figure 5, which is only an artifact [29]. The reason for this is that the build-up of the screening of the excited carriers is not accurately described by LDA in semiconductors. In contrast, metals are well described by LDA. As Si becomes metallic due to the melting, we are convinced that the behavior of the band gap due to the laser excitation is correctly described by LDA. Besides this, also experiments show a reduction of the band gap with increasing temperature.

Already in 1958, the reduction of the direct band gap was measured at very low excitations [30, 31]. In 1974, this behavior of the direct band gap was measured from 5 K up to 300 K [32]. Alex et. al. measured a decrease of the indirect band gap with increasing temperature up to 750 K [28]. In 2010, Beye et al. measured the band gap closure following an intense fs-laser excitation by probing directly the valence electrons using a free-electron laser [24]. They explained the closure by different phase transitions. In 2014, a study at high excitations produced by a fs-laser shows that the direct band gap decreases due to the fs-laser excitation [33]: First, the electronic excitation decreases the direct band gap immediately after the fs-laser excitation. Then, a further decrease was measured due to the atomic disordering. Also, the T_e-dependent DFT calculations of Silvestrelli et al. show that Si melts and becomes metallic after an intense fs-laser excitation [7]. Recently, in 2019, Medvedev et al. studied theoretically the band gap closure following a fs X-ray excitation from an X-ray free-electron laser [34] and related it to the Bragg peak behavior.

Acknowledgments: B.B. acknowledges the support by the "Promotionsstipendium des Otto-Braun Fonds" and by the "Abschlussstipendium der Universität Kassel". M.E.G. acknowledges support from the Deutsche Forschungsgemeinschaft through grant GA 465/15-2. Computations were performed on the Lichtenberg High Performance Computer (HHLR) TU Darmstadt, on the IT Service Center (ITS) University of Kassel and on the computing cluster FUCHS University of Frankfurt.

Authors contributions: B.B. performed the calculations and the analysis. Both authors discussed the results, agreed on the conclusions and wrote the paper.

References

[1] J. R. Chelikowsky and M. L. Cohen, Phys. Rev. B 10, 5095–5107 (1974).
[2] S. Minomura and H. Drickamer, J. Phys. Chem. Solids 23, 451–456 (1962).
[3] R. H. Wentorf and J. S. Kasper, Science 139, 338–339 (1963).
[4] T. Dumitrică and R. E. Allen, Phys. Rev. B 66, 081202 (2002).
[5] C. V. Shank, R. Yen and C. Hirlimann, Phys. Rev. Lett. 50, 454–457 (1983).

[6] P. Stampfli and K. H. Bennemann, Phys. Rev. B 49, 7299–7305 (1994).
[7] P. L. Silvestrelli, A. Alavi, M. Parrinello and D. Frenkel, Phys. Rev. Lett. 77, 3149–3152 (1996).
[8] M. Harb, R. Ernstorfer, T. Dartigalongue, C. T. Hebeisen, R. E. Jordan, et al., J. Phys. Chem. B 110, 25308–25313 (2006). PMID: 17165976.
[9] M. Harb, R. Ernstorfer, C. T. Hebeisen, G. Sciaini, W. Peng, et al., Phys. Rev. Lett. 100, 155504 (2008).
[10] N. D. Mermin, Phys. Rev. 137, A1441–A1443 (1965).
[11] V. Recoules, J. Clérouin, G. Zérah, P. M. Anglade and S. Mazevet, Phys. Rev. Lett. 96, 055503 (2006).
[12] P. Tangney and S. Fahy, Phys. Rev. B 65, 054302 (2002).
[13] P. Blaha, K. Schwarz, G. K. H. Madsen, D. Kvasnicka, J. Luitz, et al., WIEN2k, An Augmented Plane Wave + Local Orbitals Program for Calculating Crystal Properties. Karlheinz Schwarz, Techn. Universität Wien, Austria, ISBN 3-9501031-1-2 (2018).
[14] B. Bauerhenne, E. S. Zijlstra, A. Kalitsov and M. E. Garcia, ACS Appl. Nano Mater. 1, 6932–6937 (2018).
[15] N. S. Grigoryan, T. Zier, M. E. Garcia and E. S. Zijlstra, J. Opt. Soc. Am. B 31, C22–C27 (2014).
[16] T. Zier, E. S. Zijlstra, S. Krylow and M. E. Garcia, Appl. Phys. A 123, 625 (2017).
[17] E. S. Zijlstra, F. Cheenicode Kabeer, B. Bauerhenne, T. Zier, et al., Appl. Phys. A 110, 519–528 (2013).
[18] E. S. Zijlstra, T. Zier, B. Bauerhenne, S. Krylow, P. M. Geiger, et al., Appl. Phys. A 114, 1–9 (2014).
[19] S. Goedecker, M. Teter and J. Hutter, Phys. Rev. B 54, 1703–1710 (1996).
[20] S. Goedecker, Rev. Mod. Phys. 71, 1085–1123 (1999).
[21] E. S. Zijlstra, A. Kalitsov, T. Zier and M. E. Garcia, Phys. Rev. X 3, 011005 (2013).
[22] T. Zier, E. S. Zijlstra and M. E. Garcia, Appl. Phys. A 117, 1–5 (2014).
[23] C. Rischel, A. Rousse, I. Uschmann, P.-A. Albouy, J.-P. Geindre, et al., Nature 390, 490–492 (1997).
[24] M. Beye, F. Sorgenfrei, W. F. Schlotter, W. Wurth and A. Föhlisch, Proc. Nat. Acad. Sci. 107, 16772–16776 (2010).
[25] E. D. Murray, D. M. Fritz, J. K. Wahlstrand, S. Fahy and D. A. Reis, Phys. Rev. B 72, 060301 (2005).
[26] E. M. Bothschafter, A. Paarmann, E. S. Zijlstra, N. Karpowicz, M. E. Garcia, et al., Phys. Rev. Lett. 110, 067402 (2013).
[27] J. P. Perdew, Int. J. Quant. Chem. 28, 497–523 (1985).
[28] V. Alex, S. Finkbeiner and J. Weber, J. Appl. Phys. 79, 6943–6946 (1996).
[29] S. V. Faleev, M. van Schilfgaarde, T. Kotani, F. M. C. Léonard and M. P. Desjarlais, Phys. Rev. B 74, 033101 (2006).
[30] R. Braunstein, A. R. Moore and F. Herman, Phys. Rev. 109, 695–710 (1958).
[31] G. G. Macfarlane, T. P. McLean, J. E. Quarrington and V. Roberts, Phys. Rev. 111, 1245–1254 (1958).
[32] W. Bludau, A. Onton and W. Heinke, J. Appl. Phys. 45, 1846–1848 (1974).
[33] M. Schultze, K. Ramasesha, C. Pemmaraju, S. Sato, D. Whitmore, et al., Science 346, 1348–1352 (2014).
[34] N. Medvedev, M. Kopecky, J. Chalupsky and L. Juha, Phys. Rev. B 99, 100303 (2019).

Bionotes

Bernd Bauerhenne
Theoretical Physics II Group and Center for Interdisciplinary Nanostructure Science and Technology (CINSaT), University of Kassel, Heinrich-Plett-Str. 40, 34132 Kassel, Germany
bauerhenne@uni-kassel.de
https://orcid.org/0000-0002-3397-2290

Bernd Bauerhenne studied mathematics and physics at the University of Kassel and at the University of Luxemburg with a focus on numerics and dynamical systems in mathematics and theoretical modeling of solids in physics. Since 2012 after receiving a diploma in mathematics and a diploma in physics, he has been a scientific employee at the chair for theoretical physics at the University of Kassel. He works on the theoretical modeling and simulation of the effects caused by fs-laser excitation in matter.

Martin E. Garcia
Theoretical Physics II Group and Center for Interdisciplinary Nanostructure Science and Technology (CINSaT), University of Kassel, Heinrich-Plett-Str. 40, 34132 Kassel, Germany

Prof. Garcia studied physics at Instituto Balseiro, Bariloche, Argentina. He completed his PhD at the Freie Universität Berlin in 1992. He obtained his Habilitation in Theoretical Physics at the Freie Universität Berlin in 1999. He was an Iberdrola Fellow at the University of Valladolid (Spain) and a Ramón y Cajal Fellow at the University of the Balearic Islands (Spain). After a nonpermanent professorship at the University of Greifswald (Germany), he obtained a permanent professorship in Kassel in 2004. The main research interests of Prof. Garcia are interaction of light with matter, ultrafast phenomena, solid state physics and biophysics.